redin Revista Facultad de Ingeniería, Universidad de Antioquia, No.104, pp. 20-32, Jul-Sep 2022

Analytical performance evaluation of GFDM in underwater acoustic communication systems

Evaluación analítica de desempeño del GFDM en sistemas de comunicación acústica subacuática

Alexander Hilario-Tacuri [1*], **Leonel Soncco** [1], **Diego Donaires** [1], **Juan Borja** [1]

[1]Departamento de Ingeniería Electrónica, Universidad Nacional de San Agustín de Arequipa. Santa Catalina # 117. C. P. 04000. Arequipa, Perú.

CITE THIS ARTICLE AS:

A. Hilario-Tacuri, L. Soncco, D. Donaires and J. Borjas. "Analytical Performance Evaluation of GFDM in Underwater Acoustic Communication Systems", *Revista Facultad de Ingeniería Universidad de Antioquia*, no. 104, pp. 20-32, Jul-Sep 2022. [Online]. Available: https://www.doi.org/10.17533/udea.redin.20210741

ARTICLE INFO:

Received: August 04, 2020
Accepted: July 26, 2021
Available online: July 28, 2021

KEYWORDS:

Probability theory; GFDM; performance appraisal; telecommunications; underwater technology

Teoría de probabilidad; GFDM; evaluación de desempeño; telecomunicaciones; tecnología subacuática

ABSTRACT: The rapid growth of the Internet of Things (IoT) has extended its concept to underwater environments. However, the implementation of these systems via wired communication still represents a technological challenge, mainly due to the high cost of their deployment. Therefore, wireless communications are seen as an interesting solution for the deployment of underwater communications systems. Preliminary research indicated that underwater acoustic wireless communication could be used for some Internet of Underwater Things applications, mainly due to the wide range of communications involved. However, a significant disadvantage of acoustic systems is their low transmission data rate; thus, studies and analyses to improve this disadvantage must be carried out. Considering that new waveforms have been proposed to improve the performance of terrestrial wireless communications systems, this work presents the development of general analytical expressions that allow the performance evaluation of the Generalized Frequency Division Multiplexing (GFDM) waveform in underwater environments. These analytical expressions were obtained considering a continuous-time model for the GFDM signal and modeling the underwater acoustic communication channel as a time-varying multipath channel. Numerical results were obtained for many different systems and channel parameters, allowing a quantitative evaluation of the system performance degradation.

RESUMEN: El rápido crecimiento de Internet de las cosas (IoT) ha extendido su concepto a entornos subacuáticos. Sin embargo, la implementación de estos sistemas a través de comunicación cableada todavía representa un desafío tecnológico, principalmente debido al alto costo de su implementación. Por lo tanto, las comunicaciones inalámbricas se consideran una solución interesante para el despliegue de sistemas de comunicaciones subacuáticos. Investigaciones preliminares indican que la comunicación inalámbrica acústica subacuática se puede utilizar para algunas aplicaciones de Internet de las cosas subacuáticas, principalmente debido al amplio rango de comunicación que tiene. Sin embargo, una desventaja significativa de los sistemas acústicos es su baja velocidad de transmisión de datos, por lo tanto, se deben realizar estudios y análisis para mejorar esta desventaja. Teniendo en cuenta que se han propuesto nuevas formas de onda para mejorar el rendimiento de los sistemas de comunicaciones inalámbricas terrestres, este artículo presenta el desarrollo expresiones analíticas generales que permiten la evaluación del rendimiento de la forma de onda de Multiplexación por división de frecuencia generalizada (GFDM) en entornos subacuáticos. Estas expresiones analíticas se obtuvieron considerando un modelo de tiempo continuo para la señal GFDM y modelando el canal de comunicación acústica subacuática como un canal multitrayecto variable en el tiempo. Se obtuvieron resultados numéricos para muchos parámetros diferentes del sistema y del canal, lo que permitió una evaluación cuantitativa de la degradación del rendimiento del sistema.

* Corresponding author: Alexander Hilario-Tacuri
E-mail: ahilariot@unsa.edu.pe
ISSN 0120-6230
e-ISSN 2422-2844

DOI: 10.17533/udea.redin.20210741

1. Introduction

Recently, both academia and industry have been interested in implementing the Internet of Things (IoT) technology (commonly used in terrestrial environments) but in underwater environments [1, 2]. Some applications proposed using IoT in underwater environments include Submarine pollution monitoring [3], fish farm monitoring [4], climate change monitoring [5], and ocean data collection [6]. Mainly due to costs, wireless communications play an important role in the deployment of these applications. However, underwater wireless communications present new challenges when compared to terrestrial wireless systems. In the literature, it is possible to find some solutions to implement underwater wireless communications: Radio-Frequency communications can also be used in underwater environments, although it is possible to achieve high transmission data rates, the communication range is extremely short [7, 8]. Another solution is the use of optical communications [9, 10], which has a high transmission data rate but necessarily requires an aligned line of sight, so its use becomes unfeasible in mobile wireless systems. Finally, another solution proposed and widely studied is the use of acoustic modems [11, 12], which, although it has a relatively low transmission data rate, has a great communication range and allows total mobility of the transmitter and receiver.

Studies that can be found in the literature about acoustic modems include: Location algorithms [13, 14], channel estimation [15, 16], performance analysis [17, 18], and implementation techniques [19, 20]. At this point, it is important to note that most of these and other studies [21, 22] consider the use of the Orthogonal Frequency Division Multiplexing (OFDM) as the main waveform for transmitting the information. In recent years, new waveforms with better features than OFDM have been proposed and analyzed [23–25]. The new waveform known as Generalized Frequency Division Multiplexing (GFDM) has been considered by many researchers as the most promising, mainly due to the flexibility of this waveform. GFDM is a block-based non-orthogonal multicarrier waveform whose block is composed of M sub-symbols and N sub-carriers which are cyclically filtered by a shaping pulse that is shifted into frequency and time domains [26]. In the literature, it is possible to find several studies about GFDM that include, among others: channel estimation [27], equalization [28], receiver design [29–31], and performance evaluation [32–34]. Even with the considerable advantages of this new waveform, its application in underwater systems has been little explored. A first attempt to analyze the use of GFDM in underwater acoustic communications systems was presented in [35], where mathematical expressions of the power spectral density were derived. This work presents the derivation of general analytical expressions to evaluate the performance of the GFDM waveform operating over underwater acoustic communication channels in terms of the out-of-band emissions and the symbol error probability.

The remaining sections of this work are organized as follows. In Section 2, the system model is introduced: mathematical expressions for the GFDM transmitter, the underwater acoustic communication channel, and the GFDM receiver are presented. In Section 3, the development of analytical expressions for the out-of-band emissions and symbol error probability are presented. Using these analytical expressions, numerical results for a particular underwater acoustic communication system are obtained and presented in Section 4. Finally, conclusions are drawn in Section 5.

2. System model

2.1 GFDM transmiter

The block diagram of the GFDM transmitter continuous-time model is presented in Figure 1. According to this diagram, the GFDM symbol $\tilde{x}_k(t)$ can be expressed as presented in Equation 1 [32].

$$\tilde{x}_k(t) = \sum_{n=0}^{N-1} \sum_{m=0}^{M-1} X_{k,n,m}\, g_m(t) e^{j\frac{2\pi nt}{T_s}} \tag{1}$$

with N denoting the number of sub-carriers, M the number of sub-symbols, and T_s the symbol duration. Still in (1), $X_{k,n,m}$ represents the transmitted symbol and $g_m(t)$ the transmission filter given by the product of a windowing pulse $w(t)$ of duration $T = MT_s$ and a shifted version of a periodic shaping pulse $g(t)$, that is given by Equation 2.

$$g_m(t) = w(t)g(t - mT_s). \tag{2}$$

As presented in [32], Equation 3 shows the power spectral density (PSD) of the GFDM symbol defined in Equation 3.

$$S_{\tilde{x}_k}(f) = \frac{E_x}{T} \sum_{n=0}^{N-1} \sum_{m=0}^{M-1} \left| G_m\left(f - \frac{n}{T_s}\right)\right|^2 \tag{3}$$

where E_x represents the mean energy of the complex symbols $X_{k,n,m}$, and $G_m(f)$ denotes the Fourier transform of $g_m(t)$ (see Equation 4)

$$G_m(f) = \frac{1}{T} \sum_{i=-\infty}^{\infty} G_T(i/T) W(f - i/T) e^{-j\frac{2\pi mi}{M}} \tag{4}$$

with $W(f)$ denoting the Fourier transform of the windowing pulse $w(t)$ and $G_T(f)$ denoting the Fourier

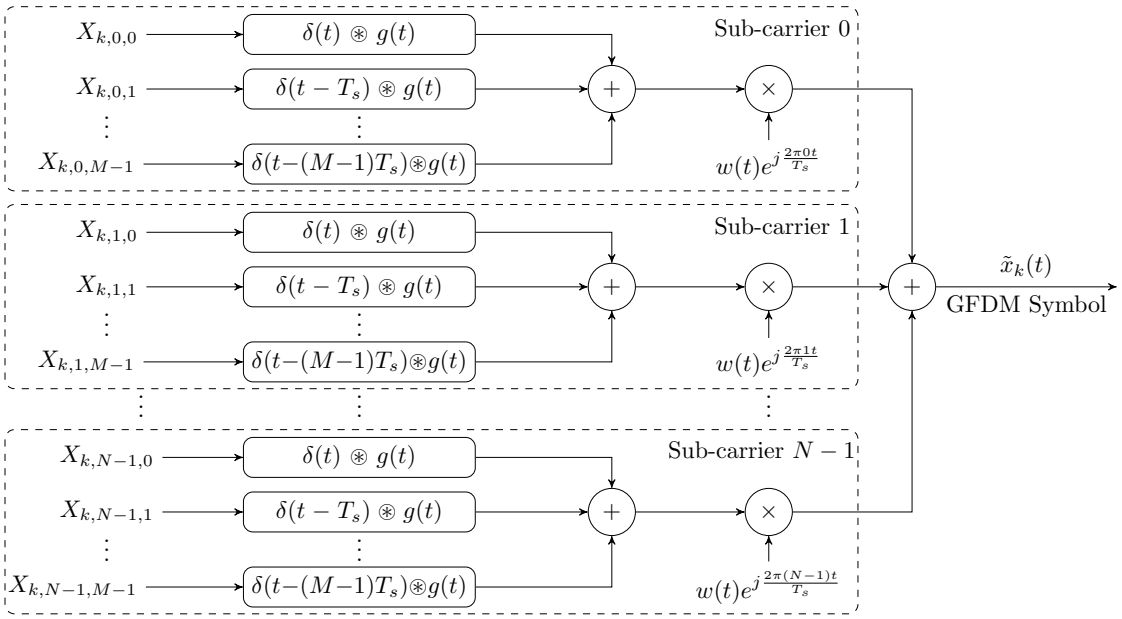

Figure 1 Continuous-time block diagram of GFDM transmitter

transform of one period of the shaping pulse $g(t)$.

Figure 2 presents the PSD of GFDM symbols for different numbers of sub-symbols. These PSDs were obtained assuming a raised cosine shaping pulse, a rectangular windowing pulse, and using (3) and (4). This figure shows that the spectral behavior of the transmitted GFDM symbol is improved when high values of M are chosen. Note that when $M = 1$, the waveform is the classic OFDM.

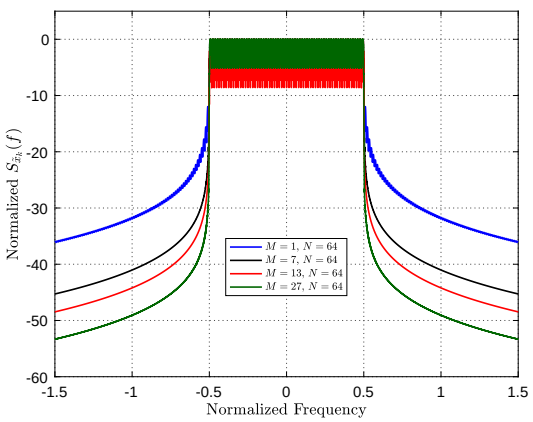

Figure 2 PSD of transmitted GFDM symbols with different numbers of sub-symbols

2.2 Underwater communication channel

Equation 5, presents the baseband impulse response of the underwater acoustic communication channel that was considered as being a time-varying multipath channel [35–38].

$$\tilde{h}(t,v) = \sum_{p=0}^{P-1} a_p \mu_p(t) \delta(v - v_p) \quad (5)$$

with a_p and v_p representing the path amplitude and the time-varying path delay, respectively. Still in (5), P represents the number of channel paths, $\mu_p(t)$ is a complex Gaussian random process with zero mean and $\delta(\cdot)$ denotes the impulse function.

Assuming that complex processes $\mu_{p_1}(t)$ and $\mu_{p_2}(t)$ are jointly wide-sense stationary and uncorrelated for $p_1 \neq p_2$, Equation 6 presents the autocorrelation function of the underwater acoustic communication channel.

$$R_{\tilde{h}}(\tau, v_1, v_2) = \sum_{p=0}^{P-1} |a_p|^2 R_{\mu_p}(\tau) \delta(v_1 - v_p) \delta(v_2 - v_p) \quad (6)$$

where $R_{\mu_p}(\tau)$ represents the autocorrelation function of the complex process $\mu_p(t)$, that is, defined by Equation 7.

$$R_{\mu_p}(\tau) = E[\mu_p(t) \mu_p^*(t+\tau)]. \quad (7)$$

2.3 GFMD receiver

In this work, the GFDM receiver is considered to be a matched filter receiver whose block diagram is presented in Figure 3. Thus, the mathematical expression of the received symbol is presented in Equation 8:

$$\hat{X}_{k,n,m} = \int_{-\infty}^{\infty} \tilde{r}_k(t) g_m^*(t) e^{\frac{-j2\pi nt}{T_s}} dt. \quad (8)$$

Where $\tilde{r}_k(t)$ is given by Equation (9):

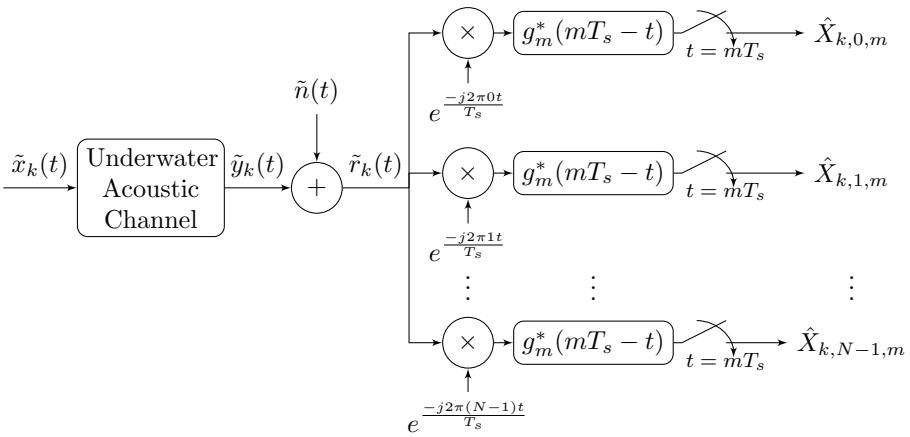

Figure 3 Continuous-time block diagram of GFDM receiver.

$$\tilde{r}_k(t) = \int_{-\infty}^{\infty} \tilde{h}(t,\tau)\tilde{x}_k(t-\tau)d\tau + \tilde{n}(t) \tag{9}$$

with $\tilde{h}(t,\tau)$ representing the impulse response of the underwater acoustic channel and $\tilde{n}(t)$ an additive white Gaussian noise (AWGN) with zero mean and variance N_0.

Using (1) in (9), a more compact version of (8) can be written as Equation 10 (See details in Appendix A):

$$\hat{X}_{k,n,m} = R_{n,m}X_{k,n,m} + I_{k,n,m} + N_{k,n,m} \tag{10}$$

where the mathematical expressions of $R_{n,m}$, $I_{k,n,m}$ and $N_{k,n,m}$ are presented in Equations 11, 12 and 13 respectively.

$$R_{n,m} = \int_{-\infty}^{\infty}\int_{-\infty}^{\infty} \tilde{h}(t,\tau)g_m(t-\tau)g_m^*(t)e^{-j\frac{2\pi n_1\tau}{T_s}}dtd\tau, \tag{11}$$

$$I_{k,n,m} = \sum_{\substack{n_1=0\\(n_1\neq n,\, m_1\neq m)}}^{N-1}\sum_{m_1=0}^{M-1} X_{k,n_1,m_1}R_{n_1,m_1}^{(n,m)}, \tag{12}$$

$$N_{k,n,m} = \int_{-\infty}^{\infty} \tilde{n}(t)g_m^*(t)e^{\frac{-j2\pi nt}{T_s}}dt. \tag{13}$$

The mathematical expression of $R_{n_1,m_1}^{(n,m)}$ in (12), is presented in Equation 14.

$$R_{n_1,m_1}^{(n,m)} = \int_{-\infty}^{\infty}\int_{-\infty}^{\infty} \tilde{h}(t,\tau)g_{m_1}(t-\tau)g_m^*(t)e^{j\frac{2\pi[t(n_1-n)-n_1\tau]}{Ts}}dtd\tau. \tag{14}$$

3. System performance

The performance evaluation of GFDM in underwater acoustic communication systems is carried out based on its out-of-band emissions (OOB_e) and symbol error probability. Thus, general analytical expressions of these performance measures are presented below.

3.1 Out-of-band emissions

The received GFDM signal can be expressed as Equation 15:

$$\tilde{y}_k(t) = \int_{-\infty}^{\infty} \tilde{h}(t,\tau)\tilde{x}_k(t-\tau)d\tau. \tag{15}$$

Using (5) in (15) and after some mathematical manipulations, $\tilde{y}_k(t)$ can be rewritten as presented in Equation 16.

$$\tilde{y}_k(t) = \sum_{p=0}^{P-1} a_p\mu_p(t)\tilde{x}_k(t-v_p). \tag{16}$$

The autocorrelation function of $y_k(t)$ defined by (17):

$$R_{\tilde{y}_k}(t,\tau) = E[\tilde{y}_k^*(t+\tau)\tilde{y}_k(t)] \tag{17}$$

can be expressed as (18):

$$R_{\tilde{y}_k}(t,\tau) = \sum_{p=0}^{P-1} |a_p|^2 R_{\mu_p}(\tau)R_{\tilde{x}_k}(t-v_p,\tau) \tag{18}$$

where $R_{\tilde{x}_k}(t,\tau)$ and $R_{\mu_p}(\tau)$ represents the autocorrelation function of $\tilde{x}_k(t)$ and $\mu_p(t)$, respectively. The mean in time of $R_{\tilde{y}_k}(t,\tau)$ is presented in Equation 19 (See details in Appendix B):

$$\bar{R}_{\tilde{y}_k}(\tau) = \lim_{T\to\infty}\frac{1}{T}\int_T R_{\tilde{y}_k}(t,\tau)dt = \sum_{p=0}^{P-1}|a_p|^2 R_{\mu_p}(\tau)\bar{R}_{\tilde{x}_k}(\tau) \tag{19}$$

and the PSD of the received GFDM signal is given by the Fourier transform of $\bar{R}_{\tilde{y}_k}(\tau)$, that is, given by Equation 20.

$$S_{\tilde{y}_k}(f) = \sum_{p=0}^{P-1} |a_p|^2 S_{\mu_p}(f) * S_{\tilde{x}_k}(f) \quad (20)$$

with $S_{\mu_p}(f)$ denoting the Fourier transform of $R_{\mu_p}(\tau)$ and $S_{\tilde{x}_k}(f)$ denoting the PSD of the transmitted GFDM symbol defined in (3). Still in (20), "$*$" denotes the convolution operator.

Finally, assuming that the useful bandwidth of the received GFDM symbol is B, Equation 21 shows the OOB_e defined as the relationship between the energy outside and inside that useful band.

$$OOB_e = \frac{\int_{f \notin B} S_{\tilde{y}_k}(f) df}{\int_{f \in B} S_{\tilde{y}_k}(f) df}. \quad (21)$$

3.2 Symbol Error Probability

Considering Equation 10, the decision variable, $D_{k,n,m}$, conditioned to a certain value of $R_{n,m} = \alpha$, can be written as Equation 22.

$$D_{k,n,m} | (R_{n,m} = \alpha) = \frac{\hat{X}_{k,n,m}}{\alpha} = X_{k,n,m} + Z_{k,n,m}(\alpha) \quad (22)$$

where (23):

$$Z_{k,n,m}(\alpha) = \frac{I_{k,n,m} + N_{k,n,m}}{\alpha}. \quad (23)$$

Then, the symbol error probability can be obtained by using Equation 24:

$$P_{n,m}(e) = \int_{-\infty}^{\infty} P_{n,m}(e|R_{n,m} = \alpha) p_{R_{n,m}}(\alpha) d\alpha \quad (24)$$

where $p_{R_{n,m}}(\alpha)$ represents the probability density function of $R_{n,m}$ and the conditional error probability of the right side of (24) depends on the digital modulation used. Expressions for this conditional error probability can be found in the literature; for instance, for PSK and QAM digital modulations, these expressions are shown in Equations 25 and 26, respectively [39].

$$P_{n,m}(e|R_{n,m} = \alpha) \approx 2Q\left(\sqrt{2\gamma_{n,m}(\alpha)} \sin\left(\frac{\pi}{\mathcal{M}}\right)\right) \quad (25)$$

$$P_{n,m}(e|R_{n,m} = \alpha) \approx 4Q\left(\sqrt{\frac{3\gamma_{n,m}(\alpha)}{\mathcal{M}-1}}\right) \quad (26)$$

In (25) and (26), $\mathcal{M}$ represents the modulation order and $\gamma_{n,m}(\alpha)$ denotes the symbol energy to noise ratio defined as Equation (27).

$$\gamma_{n,m}(\alpha) = \frac{E_x}{\sigma^2_{Z_{n,m}}(\alpha)} \quad (27)$$

with $\sigma^2_{Z_{n,m}}(\alpha)$ representing the variance of $Z_{k,n,m}(\alpha)$. Finally the overall error probability is obtained by using Equation 28:

$$P(e) = \frac{1}{N\,M} \sum_{n=0}^{N-1} \sum_{m=0}^{M-1} P_{n,m}(e). \quad (28)$$

At this point, it is good to note that (25) and (26) are only valid when $Z_{k,n,m}(\alpha)$ is a Gaussian random variable. Results demonstrating this assumption are presented below.

Statistical characterization of $Z_{k,n,m}(\alpha)$

From (12), (13) and taking into consideration the statistical characteristics of the underwater communication channel, $h(t,\tau)$, and the AWGN, $\tilde{n}(t)$, can be proved that both $I_{k,n,m}$ and $N_{k,n,m}$ not only are Gaussian random variables but also independent of each other. Thus, it is possible to conclude that $Z_{k,n,m}(\alpha)$ is also a Gaussian random variable.

The mean and the variance of $Z_{k,n,m}(\alpha)$ are presented in Equations 29 and 30, respectively.

$$E[Z_{k,n,m}(\alpha)] = \frac{E[I_{k,n,m}] + E[N_{k,n,m}]}{\alpha} = 0 \quad (29)$$

$$\sigma^2_{Z_{n,m}}(\alpha) = \frac{\sigma^2_{I_{n,m}} + \sigma^2_{N_{n,m}}}{\alpha^2} \quad (30)$$

In (29), $\sigma^2_{I_{n,m}}$ and $\sigma^2_{N_{n,m}}$ represents the variance of $I_{k,n,m}$ and $N_{k,n,m}$, respectively. From (12) is possible to shown that $\sigma^2_{I_{n,m}}$ is given by Equation 31.

$$\sigma^2_{I_{n,m}} = E_x \sum_{\substack{n_1=0 \\ (n_1 \neq n,\ m_1 \neq m)}}^{N-1} \sum_{m_1=0}^{M-1} C^{(n,m)}_{n_1,m_1} \quad (31)$$

where (32):

$$C^{(n,m)}_{n_1,m_1} = \sum_{p=0}^{P-1} |a_p|^2 S_{\mu_p}(f) * B^m_{m_1}(f)\Big|_{f=\frac{n_1-n}{Ts}} \quad (32)$$

with (33) (refer to Appendix D):

$$B^m_{m_1}(f) = \left| G^*_m(f) * G_{m_1}(-f) \right|^2. \quad (33)$$

Analogously, from (13), $\sigma^2_{N_{n,m}}$ is given by Equation 34 (refer to Appendix C).

$$\sigma^2_{N_{n,m}} = N_0 \int_{-\infty}^{\infty} |G_m(f)|^2 df. \quad (34)$$

Statistical characterization of $R_{n,m}$

From the definition of $R_{n,m}$ presented in (11), it can be shown that $R_{n,m}$ is a complex Gaussian random variable; thus, its probability density function can be written as Equation 35.

$$p_{R_{n,m}}(\alpha) = \frac{1}{2\pi\sigma^2_{R_{n,m}}} e^{-\frac{|\alpha-\mu_{R_{n,m}}|^2}{2\sigma^2_{R_{n,m}}}} \tag{35}$$

where $\mu_{R_{n,m}}$ and $\sigma^2_{R_{n,m}}$ are given by Equations 36 and 37 respectively.

$$\mu_{R_{n,m}} = E[R_{n,m}] = 0 \tag{36}$$

$$\begin{aligned}\sigma^2_{R_{n,m}} &= E[|R_{n,m}|^2] \\ &= E_x \sum_{p=0}^{P-1} |a_p|^2 \int_{-\infty}^{\infty} S_{\mu_p}(f) \left| G^*_m(-f) * G_m(f) \right|^2 df.\end{aligned} \tag{37}$$

4. Numerical results

In this section, numerical results for the OOB_e and the symbol error probability of GFDM operating over a particular underwater acoustic communication system are presented. The system under consideration uses the BPSK modulation with $T_s = 1\mu$s. In addition, the windowing pulse $w_T(t)$ is assumed to be rectangular and the periodic shaping pulse $g(t)$ is a raised cosine with roll-off factor β, meaning that $g_T(t)$ is defined as Equation 38.

$$g_T(t) = \text{sinc}(\pi t/T_s) \frac{\cos(\pi\beta t/T_s)}{1-(2\beta t/T_s)^2}; \quad t \in \left[-\frac{T}{2}, \frac{T}{2}\right] \tag{38}$$

For the underwater acoustic communication channel the time-varying multipath model presented in (5) is used with $P = 4$ and the path delays and amplitudes are assumed to be $a_0 = 0.8677$, $a_1 = 0.4339$, $a_2 = 0.2169$, $a_3 = 0.1085$, $v_0 = 0\mu$s, $v_1 = 0.2\mu$s, $v_2 = 0.4\mu$s and $v_3 = 0.6\mu$s. Still in (5), the random process $\mu_p(t)$ was considered to have Jake's PSD [40], thereby, $S_{\mu_p}(f)$ is given by Equation 39.

$$S_{\mu_p}(f) = \frac{1}{\pi f_d \sqrt{1-\left(\frac{f}{f_d}\right)^2}}; \quad |f| \leq f_d \tag{39}$$

with f_d denoting the maximum Doppler shift.

4.1 Spectral evaluation

The PSD of the GFDM received signal $\tilde{y}_k(t)$ was obtained only using (3), (20) and (39). Thus, the OOB_e of GFDM operating over the underwater acoustic communication channel was computed using (21). The effects of the number of sub-carriers and number of sub-symbols over the PSD of the received GFDM signal are shown in Figures 4 and 5, respectively. Here, the considered maximum Doppler shift was 15 Hz. Both figures confirm that the received GFDM signal has lower OOB_e when the N or M values are high. Tables 1 and 2 show the OOB_e computed values of the transmitted and received GFDM signals for different sub-carrier and sub-symbol values. At this point, it is good to highlight that the PSD of GFDM with $M = 1$ in Figure 5 also represents the PSD of classic OFDM and, as can be seen in this figure, OFDM has the lowest performance in terms of spectral efficiency.

The effect of the maximum Doppler shift typical of the underwater acoustic communication channel is presented in Figure 6. This figure shows the PSD with 64 sub-carriers, 27 sub-symbols, and for different values of f_d. In order to make comparisons, this figure also shows the transmitted GFDM signal. Computed values of these OOB_e are presented in Table 3. As expected, these results confirm that the lower the maximum Doppler shift, the lower the out-of-band emissions of the system.

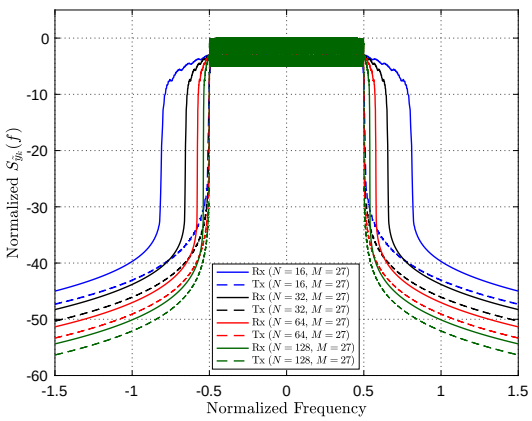

Figure 4 PSD of received GFDM signals with different numbers of sub-carriers

Table 1 OOB_e values from Figure 4

N	16	32	64	128
Tx GFDM	0.0015	0.0008	0.0004	0.0002
Rx GFDM	0.2345	0.1050	0.0499	0.0243

Table 2 OOB_e values from Figure 5

M	1	7	13	27
Tx GFDM	0.0070	0.0015	0.0010	0.0004
Rx GFDM	0.0538	0.0503	0.0500	0.0499

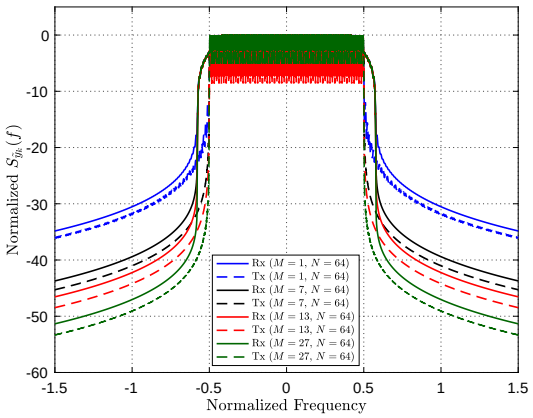

Figure 5 PSD of received GFDM signals with different numbers of sub-symbols

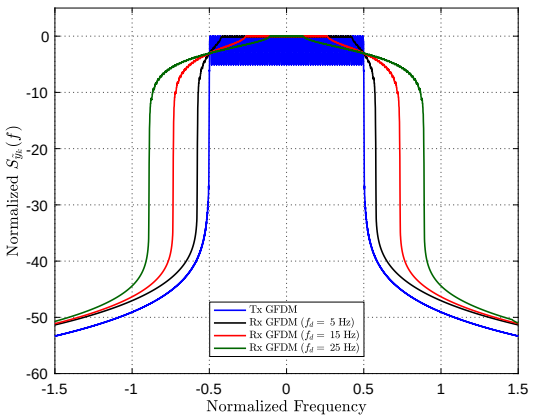

Figure 6 PSD of received GFDM signals with different values of maximum Doppler shift

4.2 Symbol error probability

The numerical results of the symbol error probability were obtained using only (24), (25), (27) and (28). The effects of the GFDM parameters (N, M, α) and the channel parameter f_d over the symbol error probability of receiver GFDM are depicted in Figures 7 - 10, respectively. In order to make comparisons, all these figures also show the error probability of the receiver GFDM corrupted only by AWGN. These figures reveal that the presence of a time-varying channel (underwater acoustic communication channel) seriously degrades the symbol error probability of the system.

Figure 7 shows the symbol error probability for an underwater system with different values of N. The other parameters of the system, this is, the number of sub-symbol, the roll-off factor and the maximum Doppler shift, were set to be 7, 0.5 and 10 Hz, respectively. As can be seen in this figure, the symbol error probability is weakly dependent on the number of sub-carriers for both, systems operating over an underwater acoustic channel and systems only corrupted by AWGN.

Table 3 OOB_e values from Figure 6

f_d	0	5	15	25
Tx GFDM	0.0004	0.0004	0.0004	0.0004
Rx GFDM	0.0004	0.0499	0.1704	0.3229

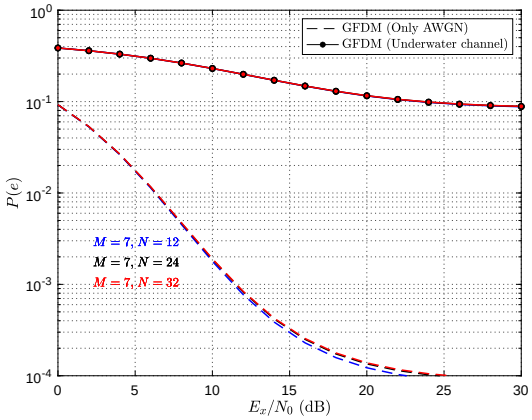

Figure 7 Symbol error probability of an underwater system using GFDM with different values of N

The symbol error probability for an underwater system with different values of M is presented in Figure 8. Here, the number of sub-carriers, the roll-off factor and the maximum Doppler shift were set to be 64, 0.5 and 10 Hz, respectively. This figure reveals that symbol error probability is strongly dependent on the total number of sub-symbols. As expected, while considering high values of M, the symbol error probability is also high. As mentioned before, the GFDM with $M = 1$ represents the classical OFDM, which in terms of symbol error probability, has the best performance. Figure 9 presents the effects of the roll-off factor α on the symbol error rate probability of an underwater system. This time the number of sub-carriers, number of sub-symbols and maximum Doppler shift were set to be 64, 7 and 10 Hz, respectively. This figure confirms that symbol error probability is strongly dependent on the excess bandwidth of the periodic shaping pulse $g(t)$. Considering low values of excess bandwidth results in low error probability values. Finally, the effects of the maximum Doppler shift on the symbol error probability are presented in Figure 9. The curves presented in this figure were obtained considering 64 sub-carriers, 7 sub-symbols and $\beta = 0.5$. From this figure, it is clear that the mobility of the receiver seriously degrades the error probability of the system.

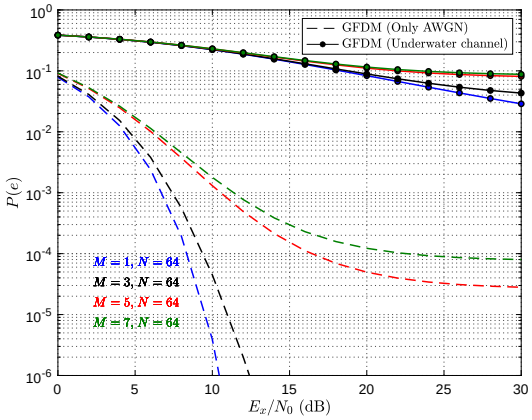

Figure 8 Symbol error probability of an underwater system using GFDM with different values of M

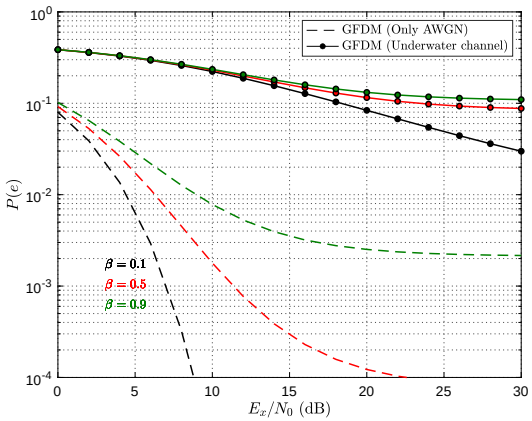

Figure 9 Symbol error probability of an underwater system using GFDM with different values of β

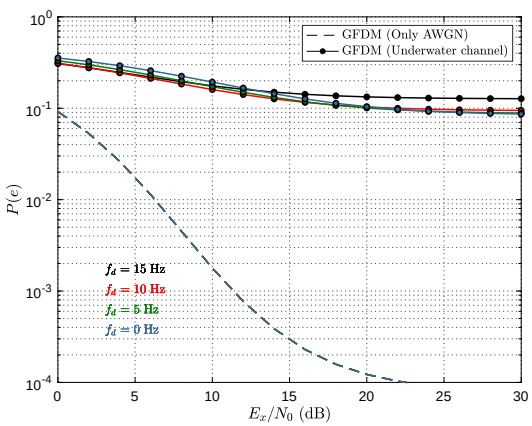

Figure 10 Symbol error probability of an underwater system using GFDM with different values of f_d

5. Conclusions

The most important contribution of this work is the derivation of analytical expressions of the symbol error probability and out-of-band emissions from underwater acoustic communications systems using the GFDM. The methodology used to obtain these analytical expressions was described in detail in Section 3. As shown in the numerical results, these expressions can easily provide curves for the power spectral density and the symbols error probability with different system parameters. The numerical results obtained show that the number of sub-symbols, number of sub-carriers, and the roll-off factor of the formatting pulse play an important role in the performance of the system, both in terms of spectral efficiency and error probability. These results also reveal that, when a matched filter receiver is used, distortions induced by underwater channels not only degrades the spectral performance of the system (e.g., increase out-of-band emissions) but also seriously increase the symbol error probability; thus, further studies on more complex receivers should be performed.

6. Declaration of competing interest

We declare that we have no significant competing interests including financial or non-financial, professional, or personal interests interfering with the full and objective presentation of the work described in this manuscript.

7. Funding

This work was derived from the research project funded by the Universidad Nacional de San Agustín de Arequipa under Contract No IBAIB-05-2019-UNSA.

8. Author contributions

Conceptualization, A.H.T. and J.B.; methodology, A.H.T.; formal analysis, A.H.T.; investigation, A.H.T, L.S., D.D and J.B.; resources, A.H.T, L.S., D.D and J.B.; writing–original draft preparation, L.S. and D.D.; writing–review and editing, A.H.T.; project administration, J.B.; funding acquisition, A.H.T and J.B. All authors have read and agreed to the published version of the manuscript.

9. Data Availability Statement

No data were used to support this study.

Appendix A: Decomposition of received symbol

Using (1) in (9), it is posible to express $\tilde{r}_k(t)$ as presented in Equation (40):

$$\tilde{r}_k(t)=\int_{-\infty}^{\infty}\tilde{h}(t,\tau)\sum_{n_1,m_1}X_{k,n_1,m_1}g_{m_1}(t-\tau)e^{j\frac{2\pi n_1(t-\tau)}{T_s}}d\tau + \tilde{n}(t) \tag{40}$$

where $\sum_{n_1,m_1}=\sum_{n_1=0}^{N-1}\sum_{m_1=0}^{M-1}$. Considering (40) and (8), the mathematical expression of the received symbol is presented in Equation (41):

$$\hat{X}_{k,n,m}=\int_{-\infty}^{\infty}\tilde{h}\,(t,\tau)\sum_{n_1,m_1}X_{k,n_1,m_1}g_{m_1}(t-\tau)e^{j2\pi\frac{n_1(t-\tau)}{T_s}}d\tau \times g_m^*(t)e^{-j\frac{2\pi nt}{T_s}}dt + \int_{-\infty}^{\infty}\tilde{n}(t)g_m^*(t)e^{-j\frac{2\pi nt}{T_s}} \tag{41}$$

By rearranging the first term of (41), it is possible to obtain Equation (42):

$$\hat{X}_{k,n,m}=\sum_{n_1,m_1}X_{k,n_1,m_1}\int_{-\infty}^{\infty}\tilde{h}\,(t,\tau)\,g_{m_1}(t-\tau) \times g_m^*(t)e^{j\frac{2\pi[t(n_1-n)-n_1\tau]}{T_s}}dtd\tau + \int_{-\infty}^{\infty}\tilde{n}(t)g_m^*(t)e^{-j\frac{2\pi nt}{T_s}}dt \tag{42}$$

Separating from the summations the term corresponding to $n_1=n$ and $m_1=m$ it is posible to write (43)

$$\hat{X}_{k,n,m}=X_{k,n,m}\int_{-\infty}^{\infty}\tilde{h}\,(t,\tau)\,g_m(t-\tau)g_m^*(t)e^{-j\frac{2\pi n\tau}{T_s}}dtd\tau + \sum_{\substack{n_1,m_1\\(n_1\neq n,m_1\neq m)}}X_{k,n_1,m_1}\int_{-\infty}^{\infty}\tilde{h}\,(t,\tau)\,g_{m_1}(t-\tau) \times g_m^*(t)e^{j\frac{2\pi[t(n_1-n)-n_1\tau]}{T_s}}dtd\tau + \int_{-\infty}^{\infty}\tilde{n}(t)g_m^*(t)e^{-j\frac{2\pi nt}{T_s}} \tag{43}$$

Defining $R_{n,m}$, $R_{n_1,m_1}^{(n,m)}$ and $N_{k,n,m}$ as presented in Equations (44), (45) and (46), respectively.

$$R_{n,m}=\int_{-\infty}^{\infty}\int_{-\infty}^{\infty}h(t,\tau)g_m(t-\tau)g_m^*(t)e^{-j\frac{2\pi n_1\tau}{T_s}}dtd\tau \tag{44}$$

$$R_{n_1,m_1}^{(n,m)}=\int_{-\infty}^{\infty}\int_{-\infty}^{\infty}h(t,\tau)g_{m_1}(t-\tau) g_m^*(t)e^{j\frac{2\pi[t(n_1-n)-n_1\tau]}{T_s}}dtd\tau \tag{45}$$

$$N_{k,n,m}=\int_{-\infty}^{\infty}\tilde{n}(t)g_m^*(t)e^{\frac{-j2\pi nt}{T_s}}dt \tag{46}$$

the received symbol $\hat{X}_{k,n,m}$ can be written as (47).

$$\hat{X}_{k,n,m}=R_{n,m}X_{k,n,m}+\sum_{\substack{n_1=0\\(n_1\neq n,}}^{N-1}\sum_{\substack{m_1=0\\m_1\neq m)}}^{M-1}X_{k,n,m}R_{n_1,m_1}^{(n,m)}+N_{k,n,m} \tag{47}$$

Finally, defining $I_{k,n,m}$ as (48)

$$I_{k,n,m}=\sum_{\substack{n_1=0\\(n_1\neq n,}}^{N-1}\sum_{\substack{m_1=0\\m_1\neq m)}}^{M-1}X_{k,n_1,m_1}R_{n_1,m_1}^{(n,m)} \tag{48}$$

$\hat{X}_{k,n,m}$ is given by Equation (49).

$$\hat{X}_{k,n,m}=R_{n,m}X_{k,n,m}+I_{k,n,m}+N_{k,n,m} \tag{49}$$

Appendix B: Autocorrelation function of $\tilde{y}_k(t)$

Using (5) in (15), it is posible to express $\tilde{y}_k(t)$ as presented in Equation (50):

$$\tilde{y}_k(t)=\int_{-\infty}^{\infty}\sum_{p=0}^{P-1}a_p\mu_p(t)\delta(\tau-v_p)\tilde{x}_k(t-\tau)d\tau \tag{50}$$

or integrating with respect to τ (51)

$$\tilde{y}_k(t)=\sum_{p=0}^{P-1}a_p\mu_p(t)\tilde{x}_k(t-v_p) \tag{51}$$

The autocorrelation function of $y_k(t)$ defined by (52):

$$R_{\tilde{y}_k}(t,\tau)=E[\tilde{y}_k^*(t+\tau)\tilde{y}_k(t)] \tag{52}$$

can be expressed as (53):

$$R_{\tilde{y}_k}(t,\tau)=\sum_{p_1=0}^{P-1}\sum_{p_2=0}^{P-1}a_{p_2}a_{p_1}^*E\Big[\mu_{p_1}^*(t+\tau)\mu_{p_2}(t)\Big] \times E\Big[\tilde{x}_k^*(t+\tau-v_{p_1})\tilde{x}_k(t-v_{p_2})\Big] \tag{53}$$

Remembering that $\mu_p(t)$ is a complex Gaussian random process with zero mean, wide-sense stationary and uncorrelated for $p_1 \neq p_2$ it is possible write Equation (54):

$$R_{\tilde{y}_k}(t,\tau) = \sum_{p=0}^{P-1} |a_p|^2 R_{\mu_p}(\tau) R_{\tilde{x}_k}(t - v_p, \tau) \tag{54}$$

Considering the Wiener-Khinchin theorem, $R_{\tilde{y}_k}(\tau)$ can be defined as shown in Equation (55)

$$\begin{aligned} R_{\tilde{y}_k}(t,\tau) &= \lim_{T\to\infty} \frac{1}{T} \int_T \sum_{p=0}^{P-1} |a_p|^2 R_{\mu_p}(\tau) R_{\tilde{x}_k}(t - v_p, \tau) dt \\ &= \sum_{p=0}^{P-1} |a_p|^2 R_{\mu_p}(\tau) \bar{R}_{\tilde{x}_k}(\tau) dt \end{aligned} \tag{55}$$

Where $\bar{R}_{\tilde{x}_k}(\tau)$ is defined in (56).

$$\begin{aligned} \bar{R}_{\tilde{x}_k}(\tau) &= \lim_{T\to\infty} \frac{1}{T} \int_T R_{\tilde{x}_k}(t - v_p, \tau) dt \\ &= \lim_{T\to\infty} \frac{1}{T} \int_T R_{\tilde{x}_k}(t, \tau) dt \end{aligned} \tag{56}$$

Note that the last equality in (56) hold in the limit $T \to \infty$.

Appendix C: Statistical Characterization of $N_{k,n,m}$

The noise after the matched filter receiver is given by (57)

$$N_{k,n,m} = \int_{-\infty}^{\infty} \tilde{n}(t) g_m^*(t) e^{\frac{-j2\pi nt}{T_s}} dt \tag{57}$$

with $\tilde{n}(t)$ representing the additive white Gaussian noise (AWGN) with zero mean and variance N_0, this is, (58) and (59)

$$E[\tilde{n}(t)] = 0 \tag{58}$$

$$E[\tilde{n}(t_1)\tilde{n}^*(t_2)] = N_0 \delta(t_1 - t_2) \tag{59}$$

The mean of $N_{k,n,m}$ is given by Equation (60):

$$\begin{aligned} E[N_{k,n,m}] &= E\left[\int_{-\infty}^{\infty} \tilde{n}(t) g_m^*(t) e^{\frac{-j2\pi nt}{T_s}} dt. \right] \\ &= \int_{-\infty}^{\infty} E[\tilde{n}(t)] g_m^*(t) e^{\frac{-j2\pi nt}{T_s}} dt \end{aligned} \tag{60}$$

Using (58), it follows that $E[N_{k,n,m}] = 0$

The variance of $N_{k,n,m}$ given by $\sigma^2_{N_{n,m}} = E[N_{k,n,m} N^*_{k,n,m}]$ is presented in Equation (61):

$$\sigma^2_{N_{n,m}} = \int_{-\infty}^{\infty}\int_{-\infty}^{\infty} E[\tilde{n}(t_1)\tilde{n}^*(t_2)] g_m^*(t_1) g_m(t_2) e^{-j\frac{2\pi n(t_1-t_2)}{T_s}} dt_1 dt_2 \tag{61}$$

considering (59) it is possible to re-write Equation (61) as (62):

$$\sigma^2_{N_{n,m}} = \int_{-\infty}^{\infty}\int_{-\infty}^{\infty} N_0 \delta(t_1 - t_2) g_m^*(t_1) g_m(t_2) e^{-j\frac{2\pi n(t_1-t_2)}{T_s}} dt_1 dt_2 \tag{62}$$

or integrating with respect to t_2 (63)

$$\sigma^2_{N_{n,m}} = N_0 \int_{-\infty}^{\infty} |g_m(t_1)|^2 dt_1 \tag{63}$$

Finally, using the Parseval's Theorem gives Equation (64):

$$\sigma^2_{N_{n,m}} = N_0 \int_{-\infty}^{\infty} |G_m(f)|^2 df \tag{64}$$

Appendix D: Statistical Characterization of $I_{k,n,m}$

The term $I_{k,n,m}$ is given by (65)

$$I_{k,n,m} = \sum_{\substack{n_1=0 \\ (n_1\neq n,\, m_1 \neq m)}}^{N-1} \sum_{m_1=0}^{M-1} X_{k,n_1,m_1} R^{(n,m)}_{n_1,m_1} \tag{65}$$

where X_{k,n_1,m_1} denote the transmitted symbols. In this article these symbols are considered to have zero mean and are statistically independent for different sub-carriers, sub-symbols and time intervals, i.e. (66) and (67).

$$E[X_{k,n,m}] = 0 \tag{66}$$

$$E\left[X_{k_1,n_1,m_1} X^*_{k_2,n_2,m_2}\right] = \begin{cases} E_x \,;\, (k_1,n_1,m_1) = (k_2,n_2,m_2) \\ 0 \,;\, (k_1,n_1,m_1) \neq (k_2,n_2,m_2) \end{cases} \tag{67}$$

The mean of $I_{k,n,m}$ is given by Equation (68):

$$\begin{aligned} E[I_{k,n,m}] &= E\left[\sum_{\substack{n_1=0 \\ (n_1\neq n,\, m_1 \neq m)}}^{N-1} \sum_{m_1=0}^{M-1} X_{k,n_1,m_1} R^{(n,m)}_{n_1,m_1} \right] \\ &= \sum_{\substack{n_1=0 \\ (n_1\neq n,\, m_1 \neq m)}}^{N-1} \sum_{m_1=0}^{M-1} E\left[X_{k,n_1,m_1}\right] E\left[R^{(n,m)}_{n_1,m_1}\right] \end{aligned} \tag{68}$$

Using (66), it follows that $E[I_{k,n,m}] = 0$.

The variance of $I_{k,n,m}$ given by $\sigma^2_{I_{n,m}} = E[I_{k,n,m}I^*_{k,n,m}]$ is presented in Equation (69):

$$\sigma^2_{I_{n,m}} = \sum_{\substack{n_1=0\\(n_1\neq n,\, m_1\neq m)}}^{N-1}\sum_{m_1=0}^{M-1}\sum_{\substack{n_2=0\\(n_2\neq n,\, m_2\neq m)}}^{N-1}\sum_{m_2=0}^{M-1} E\left[X_{k,n_1,m_1}X^*_{k,n_2,m_2}\right] \times E\left[R^{(n,m)}_{n_1,m_1}R^{*(n,m)}_{n_2,m_2}\right] \tag{69}$$

considering (67) it is possible to re-write equation (69) as (70).

$$\sigma^2_{I_{n,m}} = E[I_{k,n,m}I^*_{k,n,m}] = E_x \sum_{\substack{n_1=0\\(n_1\neq n,\, m_1\neq m)}}^{N-1}\sum_{m_1=0}^{M-1} C^{(n,m)}_{n_1,m_1} \tag{70}$$

where $C^{(n,m)}_{n_1,m_1} = E\left[\left|R^{(n,m)}_{n_1,m_1}\right|^2\right]$.

In order to compute $C^{(n,m)}_{n_1,m_1}$, it is necessary to use the definition of $R^{(n,m)}_{n_1,m_1}$ presented here in Equation (71):

$$R^{(n,m)}_{n_1,m_1} = \int_{-\infty}^{\infty}\int_{-\infty}^{\infty}\tilde{h}(t,\tau)g_{m_1}(t-\tau)g^*_m(t)e^{j\frac{2\pi[t(n_1-n)-n_1\tau]}{Ts}}dtd\tau \tag{71}$$

where $\tilde{h}(t,\tau)$ is the impulse response of the underwater communication channel with autocorrelation function given by (72)

$$R_{\tilde{h}}(\tau,v_1,v_2) = \sum_{p=0}^{P-1}|a_p|^2R_{\mu_p}(\tau)\delta(v_1-v_p)\delta(v_2-v_p) \tag{72}$$

Note that $R_{\mu_p}(\tau)$ represents the autocorrelation function of the complex process $\mu_p(t)$, that can be defined as (73)

$$R_{\mu_p}(\tau) = \int_{-\infty}^{\infty}S_{\mu_p}(f)e^{j2\pi f\tau}df \tag{73}$$

Thus, $C^{(n,m)}_{n_1,m_1}$ can be written as Equation (74):

$$C^{(n,m)}_{n_1,m_1} = \int_{-\infty}^{\infty}\cdots\int_{-\infty}^{\infty}E\left[\tilde{h}(t_1,\tau_1)\tilde{h}^*(t_2,\tau_2)\right] \times g_{m_1}(t_1-\tau_1)g^*_m(t_1)e^{j\frac{2\pi[t_1(n_1-n)-n_1\tau_1]}{Ts}} \times g^*_{m_1}(t_2-\tau_2)g_m(t_2)e^{-j\frac{2\pi[t_2(n_1-n)-n_1\tau_2]}{Ts}} \times dt_1dt_2d\tau_1d\tau_2 \tag{74}$$

or using (72)

$$C^{(n,m)}_{n_1,m_1} = \int_{-\infty}^{\infty}\cdots\int_{-\infty}^{\infty}\sum_{p=0}^{P-1}|a_p|^2R_{\mu_p}(t_1-t_2)\delta(\tau_1-v_p)\delta(\tau_2-v_p) \times g_{m_1}(t_1-\tau_1)g^*_m(t_1)e^{j\frac{2\pi[t_1(n_1-n)-n_1\tau_1]}{Ts}} \times g^*_{m_1}(t_2-\tau_2)g_m(t_2)e^{-j\frac{2\pi[t_2(n_1-n)-n_1\tau_2]}{Ts}} \times dt_1dt_2d\tau_1d\tau_2 \tag{75}$$

Integrating (75) at τ_1 and τ_2 gives equation (76):

$$C^{(n,m)}_{n_1,m_1} = \int_{-\infty}^{\infty}\cdots\int_{-\infty}^{\infty}\sum_{p=0}^{P-1}|a_p|^2R_{\mu_p}(t_1-t_2) \times g_{m_1}(t_1-v_p)g^*_m(t_1)e^{j\frac{2\pi[t_1(n_1-n)]}{Ts}} \times g^*_{m_1}(t_2-v_p)g_m(t_2)e^{-j\frac{2\pi[t_2(n_1-n)]}{Ts}}dt_1dt_2 \tag{76}$$

Using (73) and rearranging the integrals, it follows that

$$C^{(n,m)}_{n_1,m_1} = \sum_{p=0}^{P-1}|a_p|^2\int_{-\infty}^{\infty}S_{\mu_p}(f) \times \int_{-\infty}^{\infty}g_{m_1}(t_1-v_p)g^*_m(t_1)e^{-j2\pi t_1\left[-f-\frac{(n_1-n)}{Ts}\right]}dt_1 \times \int_{-\infty}^{\infty}g^*_{m_1}(t_2-v_p)g_m(t_2)e^{-j2\pi t_2\left[f+\frac{(n_1-n)}{Ts}\right]}dt_2df \tag{77}$$

Integrating (77) in t_1 and t_2 gives Equation (78):

$$C^{(n,m)}_{n_1,m_1} = \sum_{p=0}^{P-1}|a_p|^2\int_{-\infty}^{\infty}S_{\mu_p}(f) \times G_{m_1}\left(-f-\frac{(n_1-n)}{Ts}\right)*G^*_m\left(f+\frac{(n_1-n)}{Ts}\right) \times G^*_{m_1}\left(-f-\frac{(n_1-n)}{Ts}\right)*G^*_m\left(f+\frac{(n_1-n)}{Ts}\right)df \tag{78}$$

or (79)

$$C^{(n,m)}_{n_1,m_1} = \sum_{p=0}^{P-1}|a_p|^2\int_{-\infty}^{\infty}S_{\mu_p}(f) \times \left|G_{m_1}\left(-f-\frac{(n_1-n)}{Ts}\right)*G^*_m\left(f+\frac{(n_1-n)}{Ts}\right)\right|^2df \tag{79}$$

Defining the real and even function $B^m_{m_1}$ as in Equation (80):

$$B^m_{m_1}(f) = \left|G^*_m(f)*G_{m_1}(-f)\right|^2 \tag{80}$$

It is possible to re-write equation (79) as (81):

$$C^{(n,m)}_{n_1,m_1} = \sum_{p=0}^{P-1}|a_p|^2\int_{-\infty}^{\infty}S_{\mu_p}(f)B^m_{m_1}\left(f+\frac{(n_1-n)}{Ts}\right)df \tag{81}$$

Finally, using the definition of the convolution operation and remembering the $B^m_{m_1}(f)$ is an even function, we have

(82)

$$C_{n_1,m_1}^{(n,m)} = \sum_{p=0}^{P-1} |a_p|^2 S_{\mu_p}(f) * B_{m_1}^{m}(f)\Big|_{f=\frac{n_1-n}{T_s}} \quad (82)$$

References

[1] C. Kao and *et al*, "A study of applications, challenges, and channel models on the internet of underwater things," in *IEEE International Conference on Applied System Innovation (ICASI)*, Sapporo, Japan, 2017, pp. 1375–1378. [Online]. Available: https://doi.org/10.1109/ICASI.2017.7988162

[2] E. Liou and *et al*, "Internet of underwater things: Challenges and routing protocols," in *IEEE International Conference on Applied System Invention (ICASI)*, Chiba, Japan, 2018, pp. 1171–1174. [Online]. Available: https://doi.org/10.1109/ICASI.2018.8394494

[3] S. Premkumardeepak and M. Mukesh, "Intelligent sensor based monitoring system for underwater pollution," in *International Conference on IoT and Application (ICIOT)*, Nagapattinam, India, 2017, pp. 1–4. [Online]. Available: https://doi.org/10.1109/ICIOTA.2017.8073626

[4] C. Chiang, "A CMOS seawater salinity to digital converter for IoT applications of fish farms," *IEEE Transactions on Circuits and Systems I: Regular Papers*, vol. 64, no. 9, pp. 2591–2597, 2017. [Online]. Available: https://doi.org/10.1109/TCSI.2017.2686582

[5] C. A. Perez and *et al*, "Design and deployment of a wireless sensor network for the mar menor coastal observation system," *IEEE Journal of Oceanic Engineering*, vol. 42, no. 4, pp. 966–976, 2017. [Online]. Available: https://doi.org/10.1109/JOE.2016.2639118

[6] E. Fischell, T. Schneider, and H. Schmidt, "Design, implementation, and characterization of precision timing for bistatic acoustic data acquisition," *IEEE Journal of Oceanic Engineering*, vol. 41, no. 3, pp. 583–591, 2016. [Online]. Available: https://doi.org/10.1109/JOE.2015.2469975

[7] S. M. Maher and *et al*, "Performance of rf underwater communications operating at 433 mhz and 2.4 GHz," in *International Conference on Innovative Trends in Computer Engineering*, Egypt, Egypt, 2019, pp. 334–339. [Online]. Available: https://doi.org/10.1109/ITCE.2019.8646491

[8] M. Jouhari and *et al*, "Underwater wireless sensor networks: A survey on enabling technologies, localization protocols, and internet of underwater things," *IEEE Access*, vol. 7, pp. 96 879–96 899, 2019. [Online]. Available: https://doi.org/10.1109/ACCESS.2019.2928876

[9] Z. Zeng and *et al*, "A survey of underwater optical wireless communications," *IEEE Commun. Surveys Tuts.*, vol. 19, no. 1, pp. 204–238, 2017. [Online]. Available: https://doi.org/10.1109/COMST.2016.2618841

[10] H. Kaushal and G. Kaddoum, "Underwater optical wireless communication," *IEEE Access*, vol. 4, pp. 1518 – 1547, 2016. [Online]. Available: https://doi.org/10.1109/ACCESS.2016.2552538

[11] S. Sendra and *et al*, "Underwater acoustic modems," *IEEE Sensors Journal*, vol. 16, no. 11, pp. 4063–4071, 2016. [Online]. Available: https://doi.org/10.1109/JSEN.2015.2434890

[12] H. S. Dol and *et al*, "Software-defined underwater acoustic modems: Historical review and the NILUS approach," *IEEE Journal of Oceanic Engineering*, vol. 42, no. 3, pp. 722–737, 2017. [Online]. Available: https://doi.org/10.1109/JOE.2016.2598412

[13] S. Zhang and *et al*, "The localization algorithm based on symmetry correction for underwater acoustic networks," *IEEE Access*, vol. 7, pp. 121 127–121 135, 2019. [Online]. Available: https://doi.org/10.1109/ACCESS.2019.2937106

[14] D. Wang and *et al*, "Channel-adaptive location-assisted wake-up signal detection approach based on LFM over underwater acoustic channels," *IEEE Access*, vol. 7, pp. 93 806–93 819, 2019. [Online]. Available: https://doi.org/10.1109/ACCESS.2019.2926531

[15] Y. Zhou and F. Tong, "Channel estimation based equalizer for underwater acoustic multiple-input-multiple-output communication," *IEEE Access*, vol. 7, pp. 79 005–79 016, 2019. [Online]. Available: https://doi.org/10.1109/ACCESS.2019.2921596

[16] J. Zhou and *et al*, "Study of propagation channel characteristics for underwater acoustic communication environments," *IEEE Access*, vol. 7, pp. 79 438–79 445, 2019. [Online]. Available: https://doi.org/10.1109/ACCESS.2019.2921808

[17] G. Qiao and *et al*, "Analysis of snr metrics for a typical underwater acoustic OFDM system," *IEEE Access*, vol. 7, pp. 183 565–183 579, 2019. [Online]. Available: https://doi.org/10.1109/ACCESS.2019.2960304

[18] J. Li and *et al*, "Performance analysis for focused beamformers in passive underwater acoustic localization," *IEEE Access*, vol. 6, pp. 18 200–18 208, 2018. [Online]. Available: https://doi.org/10.1109/ACCESS.2018.2821766

[19] E. Demirors and *et al*, "A high-rate software-defined underwater acoustic modem with real-time adaptation capabilities," *IEEE Access*, vol. 6, pp. 18 602–18 615, 2018. [Online]. Available: https://doi.org/10.1109/ACCESS.2018.2815026

[20] Y. Zhou and F. Tong, "Research and development of a highly reconfigurable OFDM MODEM for shallow water acoustic communication," *IEEE Access*, vol. 7, pp. 123 569–123 582, 2019. [Online]. Available: https://doi.org/10.1109/ACCESS.2019.2936933

[21] R. Jiang and *et al*, "Deep neural networks for channel estimation in underwater acoustic OFDM systems," *IEEE Access*, vol. 7, pp. 23 579–23 594, 2019. [Online]. Available: https://doi.org/10.1109/ACCESS.2019.2899990

[22] J. Tao, "DFT-precoded MIMO OFDM underwater acoustic communications," *IEEE Journal of Oceanic Engineering*, vol. 43, no. 3, pp. 805–819, 2018. [Online]. Available: https://doi.org/10.1109/JOE.2017.2735590

[23] I. de Almeida and *et al*, "5G waveforms for IoT applications," *IEEE Communications Surveys & Tutorials*, vol. 21, no. 3, pp. 2554–25 679, 2019. [Online]. Available: https://doi.org/10.1109/COMST.2019.2910817

[24] Y. Tao and *et al*, "A survey: Several technologies of non-orthogonal transmission for 5G," *China Communications*, vol. 12, no. 10, pp. 1–15, 2019. [Online]. Available: https://doi.org/10.1109/CC.2015.7315054

[25] R. Gerzaguet and *et al*, "The 5G candidate waveform race: a comparison of complexity and performance," *Journal on Wireless Communications and Networking*, vol. 13, pp. 1–14, 2017. [Online]. Available: https://doi.org/10.1186/s13638-016-0792-0

[26] G. Fettweis, M. Krondorf, and S. Bittner, "GFDM - generalized frequency division multiplexing," in *IEEE 69th Vehicular Technology Conference*, Barcelona, Spain, 2009, pp. 1–4. [Online]. Available: https://doi.org/10.1109/VETECS.2009.5073571

[27] Z. Na and *et al*, "Turbo receiver channel estimation for GFDM-Based cognitive radio networks," *IEEE Access*, vol. 6, pp. 9926–9935, 2018. [Online]. Available: https://doi.org/10.1109/ACCESS.2018.2803742

[28] J. Zhong and *et al*, "Iterative frequency domain equalization for MIMO-GFDM systems," *IEEE Access*, vol. 6, pp. 19 386–19 395, 2018. [Online]. Available: https://doi.org/10.1109/ACCESS.2018.2823002

[29] H. Wang and R. Song, "Low complexity ZF receiver design for multi-user GFDMA uplink systems," *IEEE Access*, vol. 6, pp. 28 661–28 667, 2018. [Online]. Available: https://doi.org/10.1109/ACCESS.2018.2839750

[30] P. Chen, B. Su, and Y. Huang, "Matrix characterization for GFDM: Low complexity MMSE receivers and optimal filters," *IEEE Transactions on Signal Processing*, vol. 65, no. 18, pp. 4940–4955, 2017. [Online]. Available: https://doi.org/10.1109/TSP.2017.2718971

[31] S. Tiwari and S. S. Das, "Low-complexity joint-MMSE GFDM receiver," *IEEE Transactions on Communications*, vol. 66, no. 4, pp. 1661–1674, 2017. [Online]. Available: https://doi.org/10.1109/TCOMM.2017.2780854

[32] A. Hilario-Tacuri and *et al*, "Performance evaluation of generalized frequency division multiplexing systems over non-linearities with memory," *IEEE Access*, vol. 7, pp. 119 131–119 139, 2019. [Online].

Available: https://doi.org/10.1109/ACCESS.2019.2936840

[33] Z. Wang, L. Mei, X. Sha, and V. Leung, "BER analysis of WFRFT precoded OFDM and GFDM waveforms with an integer time offset," *IEEE Transactions on Vehicular Technology*, vol. 67, no. 10, pp. 9097–9111, 2018. [Online]. Available: https://doi.org/10.1109/TVT.2018.2855696

[34] Z. Wang, L. Mei, and X. Sha, "BER analysis for GFDM systems with gabor MMSE receiver," *IEEE Communications Letters*, vol. 22, no. 11, pp. 2222–2225, 2018. [Online]. Available: https://doi.org/10.1109/LCOMM.2018.2868107

[35] A. Hilario-Tacuri, "A closed-form spectral analysis of GFDM in underwater communication systems," in *2019 IEEE Latin-American Conference on Communications (LATINCOM)*, Salvador, Brazil, 2019, pp. 1–6. [Online]. Available: https://doi.org/10.1109/LATINCOM48065.2019.8937919

[36] M. J. Bocus, A. Doufexi, and D. Agrafiotis, "Performance evaluation of filterbank multicarrier systems in an underwater acoustic channel," in *27th Annual IEEE International Symposium on Personal, Indoor and Mobile Radio Communications*, Valencia, Spain, 2016, pp. 1–6. [Online]. Available: https://doi.org/10.1109/PIMRC.2016.7794717

[37] Y. Liu and *et al*, "Performance analysis of OFDM over multi-scale multi-lag channels," in *IEEE 86th Vehicular Technology Conference (VTC-Fall)*, Toronto, Canada, 2017, pp. 1–5. [Online]. Available: https://doi.org/10.1109/VTCFall.2017.8287943

[38] M. J. Bocus, A. Doufexi, and D. Agrafiotis, "Non-orthogonal multiple access (NOMA) for underwater acoustic communication," in *IEEE 86th Vehicular Technology Conference (VTC-Fall)*, Chicago, USA, 2018, pp. 1–5. [Online]. Available: https://doi.org/10.1109/VTCFall.2018.8690996

[39] J. Proakis and M. Salehi, *Digital Communications*, 5th ed. New York, USA: McGraw-Hill, 2008.

[40] M. Pätzold, *Mobile fading channels*, 1st ed. New York, USA: John Wiley & Sons, 2002.